Time-resolved dual RNA-Seq reveals extensive rewiring of lung epithelial and pneumococcal transcriptomes during early infection

Rieza Aprianto[1], Jelle Slager[1], Siger Holsappel[1] and Jan-Willem Veening[1,*]

[1]Molecular Genetics Group, Groningen Biomolecular Sciences and Biotechnology Institute, Centre for Synthetic Biology, University of Groningen, Nijenborgh 7, 9747 AG Groningen, The Netherlands.

*Correspondence to: j.w.veening@rug.nl, Tel: +31 (0)50 3632408, @jwveening

Keywords: *Streptococcus pneumoniae*, transcriptomics, dual RNA-Seq, host-pathogen interaction, adherence, lung epithelial cells

Main Points

- Early pneumococcal infection model for dual RNA-Seq has been established
- Simultaneous RNA isolation, rRNA depletion and sequencing are suitable for dual RNA-Seq
- Gene expression data of host and pathogen is presented in an online user-friendly database (http://dualrnaseq.molgenrug.nl)
- A capsular mutant revealed adherence-specific host and pathogen transcriptional changes: repression of innate epithelial immune response and activation of pneumococcal sugar importers

Graphical Abstract

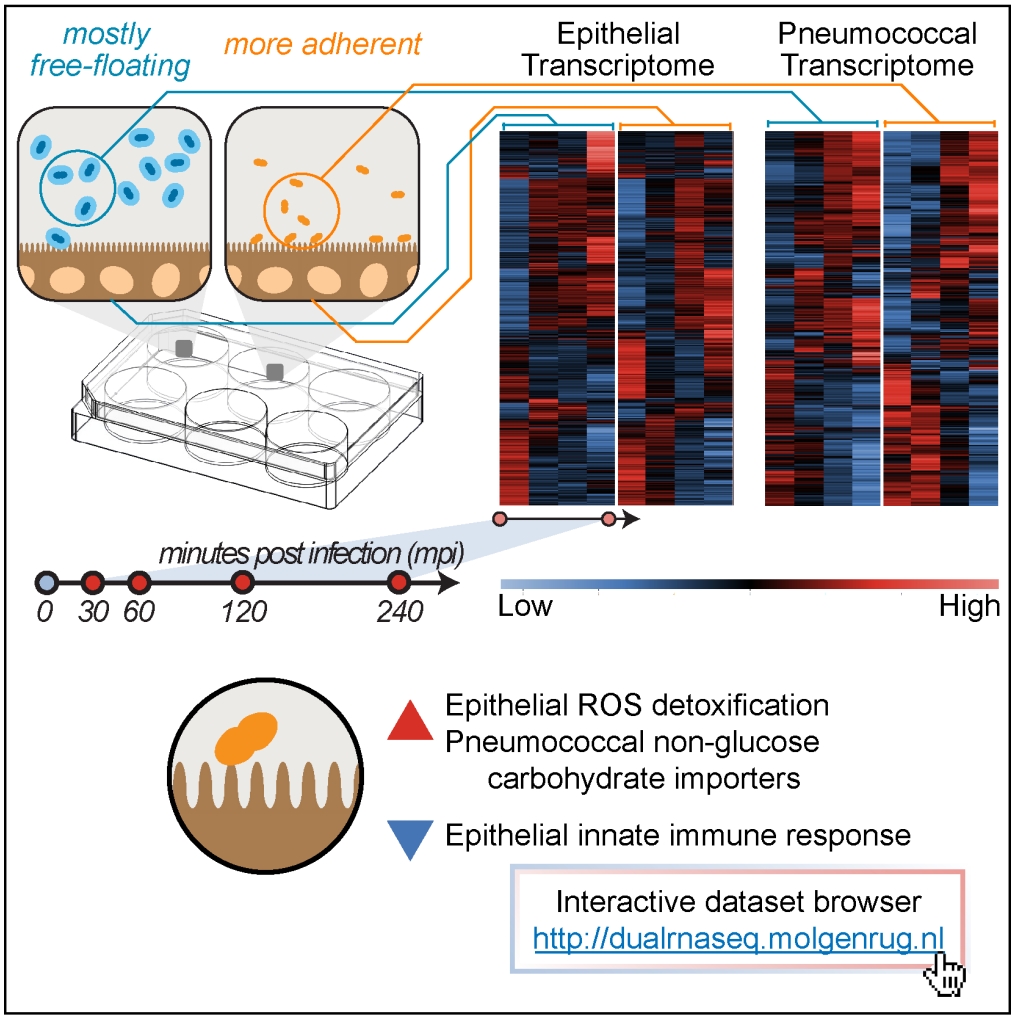

Abstract

Streptococcus pneumoniae (pneumococcus) is the main etiological agent of pneumonia. Pneumococcal pneumonia is initiated by bacterial adherence to lung epithelial cells. Infection to the epithelium is a disruptive interspecies interaction involving numerous transcription-mediated processes. Revealing transcriptional changes may provide valuable insights into pneumococcal disease. Dual RNA-Seq allows simultaneous monitoring of the transcriptomes of both host and pathogen. Here, we developed a time-resolved infection model of human lung alveolar epithelial cells by *S. pneumoniae* and assessed transcriptome changes by dual RNA-Seq. Our data provide new insights into host-microbe interactions and show that the epithelial glutathione-detoxification pathway is activated by bacterial presence. We observed that adherent pneumococci, not free-floating bacteria, access host-associated carbohydrates and repress innate immune responses. In conclusion, we provide a dynamic dual-transcriptomics overview of early pneumococcal infection with easy online access (http://dualrnaseq.molgenrug.nl). Further database exploration may expand our understanding of epithelial-pneumococcal interaction, leading to novel antimicrobial strategies.

Introduction

Lower respiratory tract infections (LRTIs), or pneumonia, claim more lives than any other communicable disease worldwide; the main etiologic agent behind this infection is the Gram-positive opportunistic pathogen *Streptococcus pneumoniae* (pneumococcus, Prina et al., 2015). Normally part of the human nasopharyngeal microflora, *S. pneumoniae* can invade the lower airways where it provokes host inflammatory and immune responses (Kadioglu et al., 2008). At the earliest stage of infection, pneumococcus adheres to epithelial cells and interacts intimately with the epithelium (Hammerschmidt et al., 2007). Meanwhile, host and pathogen cross-communicate and, they simultaneously, affect each other in a disruptive manner (Kadioglu et al., 2008; Lee et al., 2004). This interspecies interaction activates numerous processes in epithelial and pneumococcal cells (Bootsma et al., 2007; Mlacha et al., 2013). To obtain comprehensive and meaningful biological knowledge of the infection processes involved in pathogenesis, simultaneous monitoring of the transcriptome changes in both species is required (Westermann et al., 2012).

Lung epithelial cells perform vital roles during infection. First, the cells form a physical barrier to the external environment. On top of these cells, a thick layer of epithelial-derived mucus offers extra protection that traps and removes pathogens (Voynow and Rubin, 2009). Mucins, the main component of mucus, are large glycoprotein-polymers rich in sialic acids and other aminosaccharides (Rose and Voynow, 2006). Additionally, epithelial cells kill pathogens directly by producing antimicrobial peptides, e.g.: defensins and cathelicidins (Tecle et al., 2010). Moreover, epithelial cells regulate innate immune responses by secreting a wide array of pro-inflammatory cytokines, that recruit neutrophils and activate macrophages (Hallstrand et al., 2014). Finally, epithelial cells activate adaptive immune cells, including dendritic cells and T-cells via chemokine expression (Soumelis et al., 2002).

67 Pneumococcal adherence to epithelial cells is the first necessary step to
68 pathogenesis (Bogaert et al., 2004). In order to adhere, pneumococcus must quickly shed
69 the thick exopolysaccharide capsule, which protects against phagocytes (Abeyta et al.,
70 2003; Hyams et al., 2010). The shedding exposes surface adhesion factors and
71 desensitizes the bacterium from antimicrobial peptides (Beiter et al., 2008; Kietzman et al.,
72 2016). Subsequently, *S. pneumoniae* must acquire nutrients to support growth and, at the
73 same time, evade host immune responses (Shelburne et al., 2008). Pneumococcal factors
74 may be involved in multiple processes, e.g.: PsaA, a surface-exposed protein, acts
75 concurrently as adhesion factor and manganese transporter (Rajam et al., 2008). The
76 scarce manganese (Gray et al., 2010) helps in neutralizing reactive oxygen species (ROS)
77 and bacterial fitness (Tseng et al., 2002).

78 Interspecies interaction during infection is a chaotic process which necessitates rapid
79 and massive adaptation for epithelial and pneumococcal survival. During the adaptation,
80 transcriptional changes plays a focal point both in host (Jenner and Young, 2005) and in
81 pathogen (Sorek and Cossart, 2010). RNA-sequencing (RNA-Seq) delivers genome-wide
82 quantitative snapshots of the transcriptome (Kukurba and Montgomery, 2015). In a thought
83 experiment, Vogel and co-workers argued that simultaneous profiling of host and pathogen
84 transcriptomics by dual RNA-Seq might provide valuable insights for infection biology
85 (Westermann et al., 2012). Recent dual RNA-Seq studies were successful in elucidating the
86 role of sRNAs in the intracellular pathogen *Salmonella typhimurium* (Westermann et al.,
87 2016), cross-talk in the Gram-negative LRTI pathogen *Haemophilus influenzae* (Baddal et
88 al., 2015) and transcription profiles in the protozoan *Leishmania major* (Dillon et al., 2015)
89 during their respective infection.

90 Here, we exploited the dual RNA-Seq approach to simultaneously monitor the
91 transcriptome cross-talk between lung alveolar epithelial cells and pneumococci during
92 early infection. Due to the transient and highly-dynamic nature of the transcriptome
93 (Pedersen et al., 2011), we monitored the transcriptional changes in a time-resolved
94 manner. Moreover, since pneumococcal adherence to epithelial cells determines the
95 outcome of early infection, we compared adherent and non-adherent *S. pneumoniae* to
96 allow specific transcriptional interrogation on adherence. Additionally, we confirmed our
97 dual RNA-Seq gene expression data by qRT-PCR and quantitative fluorescence
98 microscopy to visualize pneumococcal proteins and thereby confirm several novel biological
99 observations identified in the dataset. Finally, we developed a user-friendly online database
100 (http://dualrnaseq.molgenrug.nl), giving access of our detailed time-resolved dual
101 transcriptomes data to the pneumococcal, microbiology, immunology and pulmonology
102 research communities.

103

104 ## Results

105 ### The early pneumococcal infection model to epithelial cells

106 At the first phase of LRTI, *S. pneumoniae* adheres to the sterile apical-side of epithelial
107 cells, adaptation of bacterial transcriptome occurs followed by bacterial outgrowth (Mlacha
108 et al., 2013), which in turn stimulate epithelial transcriptional responses to their presence
109 (Bootsma et al., 2007). We aimed to recapitulate these events in an *in vitro* model
110 consisting of co-incubation of the pathogenic *S. pneumoniae* strain D39 (serotype 2) to a
111 confluent layer of type II lung alveolar human epithelial cell (A549) at a multiplicity of
112 infection (MOI) of 10, i.e., ten pneumococci per epithelial cell (**Fig.1A**). Five time points up

113 to 4 hours after infection were selected to capture both early transcriptome responses (30
114 and 60 mpi) and later responses (120 and 240 mpi). Six technical replicates (individual
115 wells) were pooled into one biological replicate. Two biological replicates were used for
116 each time point, except for 240 mpi where we only obtained one replicate (Fig.1E). In order
117 to elucidate adherence-specific expression, we incorporated an isogenic unencapsulated
118 D39 strain (Δ*cps2E*) with increased adherence to epithelial cells into the model (Kjos et al.,
119 2015). The capsular mutant showed significantly greater capacity to adhere to epithelial
120 cells than its encapsulated parental strain ($p<0.001$, **Fig.1C**). During infection, the total
121 number of cells of both strains were significantly ($p<0.01$) increased after 4 hours (**Fig.1D**),
122 showing that both strains multiply in the model, thereby recapitulating one of the
123 characteristics of infection. To minimize transcriptional changes because of sample
124 handling, we did not separate cellular mixtures before total RNA isolation (epithelial cells,
125 adherent pneumococci and free-floating pneumococci, **Fig.1E**, see **Supplementary**
126 **Information**).

127 To analyze the time-resolved dual RNA-Seq dataset, a combination of freely
128 available bioinformatics tools was used (**Fig.1F**). First, raw reads were trimmed (Bolger et
129 al., 2014) and aligned (Dobin et al., 2013) to a chimeric genome containing the
130 concatenated genome of *Homo sapiens* (GRCh38, Ensembl) and *S. pneumoniae* D39
131 (NC_008533.1, NCBI). The one-step mapping was chosen to minimize rates of false
132 negatives. Reads were then separately counted (Liao et al., 2014) and classified as either
133 epithelial or pneumococcal. Following differential gene expression analysis, three groups of
134 genes were removed (see below) and unbiased automatic clustering (Kumar and E.
135 Futschik, 2007) and functional enrichment were performed (Dennis et al., 2003; van
136 Opijnen and Camilli, 2012).

137
138 **Dual RNA-Seq generates high-quality datasets with clusters of epithelial and**
139 **pneumococcal co-expressed genes**

140 Dual RNA-seq generated single end 75 nt reads. We sequenced to such depth, that on
141 average each library has 70 million reads (30 to 95 million). After adapter trimming and
142 removal of low-quality reads, we retained 92% (89.0-93.0%). Subsequently, 79% of reads
143 (74.6 to 83.0%) successfully aligned to the chimeric genome. Additionally, we concluded
144 that dual rRNA depletion was successful since only 0.03% of human and 0.24% of
145 pneumococcal reads mapped as ribosomal RNAs. For each library, we counted 18 million
146 epithelial reads (26%) and 37 million pneumococcal reads (52%, **Fig.2A**). The high number
147 of reads in each library and the high fraction of usable reads highlights the quality and
148 suitability of our approach for dual RNA-Seq: simultaneous total RNA isolation, dual rRNA
149 depletion and cDNA library preparation. PCA analysis showed no evidence for batch effects
150 (**Supplementary Figure 1**). Relative enrichment of pneumococcal reads may stem from
151 the total RNA isolation protocol. Nevertheless, each library contained sufficient epithelial
152 reads for differential gene expression analysis (The ENCODE Consortium, 2011).

153 To simplify further analyses, we excluded three gene fractions (**Fig.2B**). First, we
154 removed unexpressed genes, i.e., without any counts in all libraries: 22.991 (38%) epithelial
155 genes and 24 (1%) pneumococcal genes. The relatively large fraction of unexpressed
156 epithelial genes is in accordance with recent studies on the human epithelial transcriptome
157 (Hackett et al., 2012; St-Pierre et al., 2013). Second, we excluded genes that were
158 differentially expressed ($p<0.05$) at 0 mpi between unencapsulated (Δ*cps2E*) and
159 encapsulated (wt) libraries. While only five epithelial genes were removed, 394 (19%)
160 pneumococcal genes were already differentially expressed at 0 mpi. Although polar effect
161 due to *cps2E* disruption can explain differential expression of genes in the 17kb long *cps*

162 operon, it remains unknown why other genes were differentially expressed. We speculate
163 that constructing the thick exopolysaccharide capsule requires specific transcriptional fine-
164 tuning of numerous genes outside the *cps* locus. Finally, we removed genes with no
165 significant difference (p>0.05) and genes with fold changes less than 2 in all contrasts
166 (**Supplementary Figure 2**). In total, the epithelial working libraries contained 4.009 (7% of
167 total) genes and pneumococcal working libraries 868 (42% of total) genes.

168 To compare gene expression, we normalized expression values using DESeq2
169 (Love et al., 2014), centered and clustered the values (Kumar and E. Futschik, 2007). The
170 centered normalized values were visualized as heat maps, divided into two panels, one for
171 each bacterial strain. Strikingly, heat maps showed obvious clusters of co-expressed genes
172 and clear gene expression differences between adhering (Δ*cps2E*) and non-adhering (wt)
173 bacteria to epithelial cells (**Fig.2CD**). Specifically, the left panel of **Fig.2C** shows the
174 epithelial transcriptional response exposed to encapsulated *S. pneumoniae* at different time
175 points (30, 60, 120 and 240 mpi) while the right panel displays the response in contact with
176 the unencapsulated strain. *Vice versa*, co-expressed clusters in pneumococcal genes are
177 differentially expressed in contact with human epithelial cells (**Fig.2D**).

178 Making raw data publicly-available has been common practice in recent years, as we
179 have done for this project (GEO accession number GSE79595). Unfortunately, publicly
180 available datasets do not translate to direct exploration and extraction of biological insights
181 for the majority of researchers. Therefore, we built an easily-accessible online platform
182 which hosts the complete dual RNA-Seq database. To access and visualize the data, users
183 can simply select the gene of interest (or multiple genes of interests) and examine their
184 expression during early infection (**Supplementary Figure 3**). Expression data can be
185 downloaded and opened in common spreadsheet software e.g.: Microsoft Excel®. To

186 visualize expression, users can choose from three normalization methods: DESeq2
187 normalization (Love et al., 2014), TPM (transcript per million, Wagner et al., 2012) and
188 $\log_2$ -transformed TPM values.

189

190 **Validation of dual RNA-Seq by qRT-PCR and pneumococcal protein fusions**

191 To confirm dual RNA-Seq data by quantitative real-time PCR (qRT-PCR), we chose 10
192 epithelial genes (*ABCC2, AKR1B10, AKR1C3, ALDH1A1, DEFB1, DKK1, IDH1, NOLC1,*
193 *PTGES* and *TXNRD1*) and 19 pneumococcal genes (*amiC, blpY, dinF, hrcA, infC, lytA,*
194 *malC, manL, msmR, nrdD, pulA,* SPD_0249, SPD_0392, SPD_0475, SPD_0961,
195 SPD_0990, SPD_1517, SPD_1711 and SPD_1798). The target genes were selected
196 because of their varied expression profiles: increasing, decreasing or unchanged. The cycle
197 threshold (Ct) for epithelial transcripts were normalized against *ACTB* (β-actin) while
198 pneumococcal transcripts were normalized to *gyrA* (gyrase A). The reference genes were
199 highly expressed and did not show significant changes (p>0.05, FC<2) between any time
200 points during early infection. The qRT-PCR fold change was calculated by the ΔΔCt method
201 (Livak and Schmittgen, 2001) to one time point. Fold changes obtained by qRT-pCR and
202 dual RNA-Seq showed a relatively high correlation for both species: epithelial transcripts,
203 (R^2=0.72) and pneumococcal transcripts, (R^2=0.73, **Fig.3A**), validating the reliability of dual
204 RNA-Seq data.

205 Since transcript levels do not necessarily correspond with protein expression (Ning
206 et al., 2012; Taniguchi et al., 2010), we quantified four pneumococcal protein levels whose
207 genes showed upregulation during adherence to epithelial cells. We fused a fast-folding
208 variant of the green fluorescent protein (GFP) to the carboxy-termini of SPD_0475,
209 SPD_0963, SPD_1711 and SPD_1716, at their own locus while preserving all upstream

210 regulatory elements (**Fig.3B**). We transformed these constructs into the *hlpA_hlpA-rfp,*
211 Δ*cps2E* genetic background (Kjos et al., 2015). SPD_0475 encodes a 204 amino acids (aa)
212 CAAX amino terminal protease with unknown function. SPD_0963 encodes a 45 aa
213 hypothetical protein. SPD_1711 (132 aa) was described as a single stranded DNA binding
214 protein and may assist in competence (Attaiech et al., 2011) and SPD_1716 is a 63 aa
215 ortholog of cell wall or choline binding protein in other *Streptococcaceae.*

216 We imaged adherent *S. pneumoniae* with fluorescence microscopy during the
217 indicated time points (**Fig.3C**). Since (i) RFP serves as an accurate proxy for cell number
218 and viability (Kjos et al., 2015), (ii) *hlpA* does not change during early infection ($p>0.05$,
219 $FC<2$) and (iii) ratio between the GFP and RFP indicates relative expression of the protein
220 of interests (red circle and line, **Fig.3D**), we were able to quantify the proteins of interest.
221 Gene expression values from the dual RNA-Seq data (blue circles and line, **Fig.3D**) show a
222 degree of correlation with protein level in three out of the four cases – suggesting that
223 pneumococcal transcriptional changes reflects, to some extent, changes in protein level
224 (Vogel and Marcotte, 2012).

225

226 **Pneumococcal ROS induces expression of glutathione-mediated detoxification**
227 **genes in epithelial cells**

228 Along with pneumococcal adherence and multiplication, we aimed to recapitulate the host
229 response in our model. We hypothesized that the epithelial transcriptome adapts in
230 response to bacterial presence, independent of adherence. To identify the responsive
231 genes, we automatically clustered epithelial working libraries exposed to wild type
232 pneumococci. 242 epithelial genes were co-expressed in a similar manner (**Fig.4A**), i.e.,
233 lowly expressed at 30 mpi then sustained upregulation thereafter. Gene ontology (GO)

234 enrichment (Dennis et al., 2003) indicated that 26 of the subset are associated with
235 oxidation and reduction (p=5.7·10^{-4}). Moreover, 9 genes are associated directly with
236 glutathione, an ubiquitous antioxidant: *GCLC* and *GCLM*, in glutathione biosynthesis; *GPX2*
237 and *MGST2* in detoxification; and *GSR*, *IDH1*, *IDH2*, *PGD* and *G6PD* in glutathione
238 recycling.

239 Glutathione, a tripeptide of glutamic acid, cysteine and glycine, is produced and
240 secreted by epithelial cells (Valko et al., 2007). The vital molecule is biosynthesized through
241 amino-acid polymerization and when subjected to ROS (hydrogen peroxide, lipid
242 superoxide or oxygen radicals), glutathione readily donates an electron or hydrogen atom to
243 quench the ROS. The process is assisted by ligands and glutathione peroxidase (GPX2).
244 Oxidized glutathione can be recycled by glutathione reductase (GSR) dependent on
245 NADPH (**Fig.4B**). Alternatively, glutathione conjugates and neutralize ROS (Forman et al.,
246 2009). Expression of nine glutathione-associated genes showed a sustained significant
247 increase in epithelial cells exposed to encapsulated strain (p<0.05, 60 vs. 30 mpi, **Fig.4C**).

248 To validate the abovementioned finding, we repeated the experiment, isolated total
249 RNA and performed qRT-PCR on four genes: *GPX2*, involved in detoxification and *GSR*,
250 *IDH1* and *PGD*, in glutathione recycling. As expected, we observed significant upregulation
251 of these genes between 30 and 60 mpi (**Fig.4D**). Interestingly, Rai et al (2015) showed that
252 pneumococcal supernatant is sufficient to instigate oxidative damage in A549. Indeed,
253 when epithelial cells were incubated with filtered pneumococcal supernatants, the genes
254 were activated (**Fig.4D**). To establish that pneumococci-derived ROS was behind the
255 response, we added the antioxidant, resveratrol (100 μM) to the epithelial-pneumococcal
256 model and did not observe activation (**Fig.4D**) as shown by (Zahlten et al., 2015).

257

258 **Adherent *S. pneumoniae* repress epithelial innate immune response**

259 Contrasting epithelial gene expression in response to encapsulated and unencapsulated
260 pneumococci allowed us to specifically identify adherence-responsive genes. In doing so,
261 we identified 271 adherence-responsive (p<0.05) epithelial genes, of which 25 genes are
262 activated (fold change, *FC*>2) and 248 repressed (*FC*>2) during early-infection (**Fig.5A**).
263 Two genes, *PTGS2* and *HIST1H4B* showed repression and activation at more than one
264 time point. Subsequently, GO-term enrichment in the subset of repressed genes at 60 mpi
265 showed that "immune response" to be enriched in 16 genes ($p=2.3\cdot10^{-4}$, **Fig.5B**).

266 *CXCL8* (*IL8*), encoding interleukin-8, was one of the repressed immunity gene.
267 CXCL8 is a potent chemoattractant for neutrophil and other granulocytes. Interestingly, at
268 60 mpi, Δ*cps2E*-exposed epithelial cells, expressed 2.5±1.3 less *CXCL8* than epithelial
269 cells exposed to wild type *S. pneumoniae* (**Fig.5C**). This difference was validated by qRT-
270 PCR (**Fig.5D**). Further, we asked whether *CXCL8* repression is an active process or merely
271 mediated by physical adherence. To assess this, we co-incubated heat-inactivated Δ*cps2E*
272 and heat-inactivated wild type with epithelial cells. Note that heat inactivation preserves
273 pneumococcal epitope and protein structures (Hvalbye et al., 1999). *CXCL8* was still
274 significantly repressed by dead Δ*cps2E* but not by dead wild type pneumococci (**Fig.5D**) –
275 suggesting that *CXCL8* repression is independent of viability but dependent to presence of
276 the capsule or to the accessibility of surface-exposed (protein) factors in capsule absence.
277 Intriguingly, Graham and Paton (2006) showed that epithelial interleukin-8 production and
278 release was suppressed by pneumococcal surface protein CbpA and incubation with Δ*cbpA*
279 leads to higher CXCL8 expression. We speculate that the absence of capsule in Δ*cps2E*
280 increases accessibility of pneumococcal surface-exposed factors, including CbpA to
281 epithelial receptors, leading to repression of *CXCL8*.

282 *DEFB1*, encoding β-defensin-1 an important epithelial-derived constitutively-
283 expressed antimicrobial peptide (Krisanaprakornkit et al., 1998), is another repressed
284 immunity gene. However, in our model, *DEFB1* was repressed 3.0±1.2 times ($p<0.05$, 60
285 mpi) in Δ*cps2E*-exposed epithelial cells compared to wild type-exposed cells (**Fig.5C,**
286 validated in **Fig.5D**). Additionally, while heat-inactivated wild type pneumococci stimulate
287 comparable levels of *DEFB1* compared to viable wild type bacteria, non-viable Δ*cps2E*
288 repressed *DEFB1* expression even lower ($p<0.05$) than viable Δ*cps2E* (**Fig. 5D**). We
289 conclude that *DEFB1* expression is affected by adherence, accessibility of pneumococcal
290 surface proteins and pneumococcal viability by an as of yet unknown mechanism. In
291 summary, we show that adherent pneumococci modulate epithelial expression of innate
292 immunity genes, including *CXCL8* and *DEFB1*, mediated by pneumococcal surface factors.

293

294 **Adherent *S. pneumoniae* activate sugar-importers**

295 Consistent to the epithelial analysis, we contrasted pneumococcal gene expression
296 between unencapsulated and encapsulated libraries, resulting in 248 differentially
297 expressed ($p<0.05$) genes. Specifically, 110 pneumococcal genes of the 248 were
298 activated (*FC*>2) in the unencapsulated strain while 133 genes were repressed (*FC*>2,
299 **Fig.6A**). Five genes, SPD_0188, SPD_0226, SPD_0415, SPD_1717 and SPD_1988,
300 showed repression and activation at different time points. We used gene classes developed
301 for *S. pneumoniae* TIGR4 (van Opijnen and Camilli, 2012) to categorize adherence-
302 responsive genes (**Fig.6B**). Excitingly, most of the adherence-responsive genes are of
303 unknown function (133 of 248 genes, 54%), highlighting our paucity of knowledge in
304 pneumococcal gene function. A large part of the subset (36 genes, 15%) are involved in
305 cellular transport (**Fig.6B**). Since the pneumococcal genome has an exceptionally high

306 number of carbohydrate transporters (Bidossi et al., 2012), it is not surprising that 15 of the
307 genes encode for sugar transporters (**Fig.6C**).

308 At 60 mpi, 11 carbohydrate transporters were differentially expressed ($p<0.05$,
309 $FC>2$) between Δ*cps2E* and encapsulated pneumococci exposed to epithelial cells. In the
310 presence of high glucose ($2g \cdot L^{-1}$), Δ*cps2E* expressed 1.5 fold less *manLM,* encoding
311 glucose transporters, than encapsulated *S. pneumoniae* (**Fig.6D**). Moreover, seven
312 importers were activated in the adherent strain compared to the free-floating encapsulated
313 strain. The seven non-glucose transporter-genes and their substrates are SPD_0089
314 (disaccharides: galactose, mannose, N-acetylmannosamine), *celC* (disaccharides:
315 cellobiose, gentiobiose), SPD_0232/33/34 (disaccharides: cellobiose), *rafE*
316 (oligosaccharides: raffinose, stachyose, melliobiose) and *malD* (polysaccharides:
317 maltotitriol, maltodextrine, glycogen, **Fig.6D**). At the same time, four genes were repressed
318 in unencapsulated *S. pneumoniae* exposed to human epithelial cells, *glpF* (glycerol) and
319 SPD_0740/41/42 (ribonucleosides). We selected three transporter-genes, *malD*
320 (polysaccharides), *rafE* (oligosaccharides) and SPD_0234 (disaccharides) and validated
321 the abovementioned observations by qRT-PCR (**Fig.6E**).

322 Our data indicate that adherent unencapsulated bacteria detect non-glucose sugars
323 in their immediate vicinity. Epithelial mucus may provide non-glucose carbohydrates
324 (Yesilkaya et al., 2008) and simultaneously limit the interaction of epithelial cells to
325 encapsulated wild type bacteria (Nelson et al., 2007). We, then, removed epithelial-
326 associated mucus by washing the surface with warm PBS and observed that the genes
327 were no longer activated ($FC<2$, **Fig.6E**). Next, we incubated pneumococcal strains with
328 type III porcine mucin ($5\ g \cdot L^{-1}$), mimicking complex carbohydrate in the medium.
329 Interestingly, the importers were not differentially expressed between strains ($FC<2$),

330 indicating similar access to non-glucose sugars (**Fig.6E**). We conclude that following
331 adherence, *S. pneumoniae* senses an enriched host-derived non-glucose carbohydrate and
332 in turn, activates transporters to import the now-available sugars.

333

334 Discussion

335 Early infection is a chaotic and disruptive encounter between host and pathogen. In both
336 species, a multitude of transcriptional-mediated cellular processes are fine-tuned: activated,
337 maintained and repressed to ensure survival. The recently-described dual RNA-Seq
338 approach allows simultaneous host-pathogen monitoring during their interactions (Baddal et
339 al., 2015; Dillon et al., 2015; Westermann et al., 2016). In this study, we exploited the dual
340 RNA-Seq approach by application to a pneumococcal infection model to human lung
341 alveolar epithelial cells. We have generated a detailed time-resolved dataset of epithelial-
342 pneumococcal transcriptomes up to 4 hours after infection. Moreover, we have validated
343 the rich dataset by qRT-PCR and quantitative fluorescence microscopy. Furthermore, we
344 have shown that adherence-specific transcriptional responses in host and pathogen can be
345 identified by contrasting the transcriptomes of the encapsulated libraries with its
346 unencapsulated counterpart.

347 Our early-infection model recapitulated three major *in vivo* characteristics of
348 pneumococcal infection: pneumococcal adhesion, bacterial multiplication and epithelial
349 responses to pathogenic burden. Our model recapitulated these infection characteristics: (i)
350 adherence for both encapsulated and unencapsulated pneumococci (**Fig.1**), (ii)
351 pneumococcal viability and growth during early infection, e.g.: generation of ROS,
352 expression of carbohydrate importers (**Figs.4** and **6**) and (iii) host response to
353 pneumococcal presence, e.g.: glutathione-associated detoxification and innate immune

354 response (**Figs.4** and **5**). Further, as shown by regulation of carbohydrate transporters
355 (**Fig.6**), pneumococci sensed epithelial presence and subsequently adapted their
356 transcriptome.

357 Remarkably, we observed almost all (99%) pneumococcal genes are expressed at
358 early infection (**Fig.2**) – in line with recent studies on bacterial transcriptomes adapting to
359 multiple conditions (Kröger et al., 2013; Nicolas et al., 2012). We speculate that
360 interspecies interaction necessitates massive pneumococcal transcriptional adaptation.
361 Moreover, we have observed activation of detoxification genes (*GPX2* and *GSR*) in
362 epithelial cells protecting against pneumococci-derived ROS (**Fig.4**). Indeed, *S.*
363 *pneumoniae* has been reported to secrete high levels of peroxides as a by-product of its
364 pyruvate metabolism (Carvalho et al., 2011) and has recently been shown to cause DNA-
365 damage-dependent apoptosis in alveolar lung epithelial cells (Rai et al., 2015). In addition,
366 pneumococcal early competence genes (Martin et al., 2000) were activated in our model
367 (http://dualrnaseq.molgenrug.nl competence subset). Future work should also examine
368 whether small non-coding RNAs play a role in pneumococcal early infection as they do in
369 Salmonella (Westermann et al., 2016), something that was not explored currently due to the
370 poor D39 genome annotation in this regard.

371 Our approach can be expanded further by incorporating relevant LRTI agents into
372 the model. For example, alveolar macrophages and epithelial cells, together, form
373 epithelium lining of the lower respiratory tract. The cells reciprocally influence cellular
374 phenotypes and behaviors (Hussell and Bell, 2014), highly relevant to infection. Moreover,
375 pneumococcal co-infection and secondary infection are not unheard of. Influenzae virus
376 potentiates *S. pneumoniae* by neuraminidase activity that exposes cryptic epithelial
377 receptor and facilitates pneumococcal adherence (Siegel et al., 2014). In addition,

378 influenzae infection causes loss of superficial epithelial cells, revealing basal epithelium
379 (Kash et al., 2011) and aggravating secondary pneumococcal infection. On the other hand,
380 *H. influenzae* negatively affects pneumococci by recruiting neutrophils and stimulating the
381 killing of opsonized pneumococci (Lysenko et al., 2010). Incorporation of other agents into
382 the model and exploiting dual (or triple, quadruple) RNA-Seq approaches may provide
383 novel insights into respiratory infection.

384 However, complementary approaches, are needed to obtain a full picture of early
385 infection. Though transcriptome rewiring is a focal point during interspecies interaction
386 (Jenner and Young, 2005; Sorek and Cossart, 2010), non-transcriptional regulation plays
387 an important part during early infection. Capsule shedding, a hallmark of pneumococcal
388 infection, is regulated by autolysin-A (Lyt-A). LytA is activated when the bacterium
389 encounters alveolar cathelicidin (Kietzman et al., 2016), which is independent of
390 transcriptional regulation. Heterogeneity of cellular responses is another confounding factor
391 (Jørgensen et al., 2013). Recently, dual RNA-Seq combined with cell sorting was used to
392 identify heterogeneous activity of Salmonella virulence factor that, in turn, drives
393 heterogeneous interferons response in macrophage (Avraham et al., 2015). This highlights
394 the relevance of noise in gene expression and cell-to-cell variability in host-pathogen
395 interaction. Furthermore, whole organism infection models offers a more systemic
396 perspective. Dual RNA-Seq approach has been used to monitor infection in wheat-bacteria
397 (Camilios-Neto et al., 2014) and mosquito-filaria (Choi et al., 2014). Whole organism dual
398 RNA-Seq is not without its challenges, including averaging (host) effects to gene
399 expression across all cell types.

400 Besides its relevance in communicable diseases, gained insights into pneumococcal
401 infection are also applicable to understanding several non-communicable respiratory

402 diseases. Asthma, the most common chronic respiratory disease is a major risk factor for
403 pneumococcal infection (Talbot et al., 2005). Additionally, COPD (Chronic Obstructive
404 Pulmonary Disease, Decramer et al., 2012) and cigarette smoking (Phipps et al., 2010)
405 have been reported to increase the risk of pneumococcal LRTI. Here, we reported the first
406 study to show simultaneous transcriptomic changes of the pathogen *S. pneumoniae* and
407 human lung alveolar epithelial cells during early infection. Additionally, we have made the
408 time-resolved dual transcriptomics dataset available to the broader research community
409 (http://dualrnaseq.molgenrug.nl). We invite pneumococcal researchers to use the database
410 to formulate research questions in the development of preventive and curative strategies
411 against pneumococcal infection. To conclude, we call researchers from the fields of
412 microbiology, immunology and pulmonology to access the dataset and use it to develop
413 their own hypotheses.

414

415 ## Methods

416 **Culture of epithelial cell line, *S. pneumoniae* D39 and pneumococcal transformation**

417 Human type II lung epithelial cell line, A549 (ATCC® CCL-185) and *S. pneumoniae* D39
418 were routinely cultured without antibiotics. Strain construction is described in detail in
419 **Supplementary information**. Oligonucleotides are listed in **Supplementary Table 1** and
420 strains in **Supplementary Table 2**.

421 **Infection studies**

422 Confluent monolayer of A549 was co-incubated with *S. pneumoniae* D39 at multiplicities of
423 infection 10, in 1% fetal bovine serum in RPMI1640 without phenol red. Prior to infection,
424 epithelial monolayer was kept for 10 more days after confluence. To optimize cell-to-cell
425 contact, centrifugation was employed (2000 ×g, 5 min, 4°C). Adherence assays were

426 performed by enumeration of plated cfu in blood agar. More in **Supplementary**
427 **information**.

428 **Simultaneous total host-pathogen RNA isolation**

429 Before RNA isolation, samples were treated by saturated ammonium sulfate solution
430 (Korfhage et al., 2002). Cells were disrupted by bead beating, and total RNA was isolated
431 as described in the **Supplementary information**.

432 **Library preparation, sequencing, data pipeline and online database**

433 Total RNA was dual rRNA-depleted, reverse-transcribed and sequenced on the Illumina
434 NextSeq 500 in 75 nt single end mode. Raw reads were trimmed, aligned into chimeric
435 human-pneumococcus genome. Reads were counted and differential gene expression
436 analysis were performed to epithelial and pneumococcal libraries separately. Automatic
437 clustering and GO enrichment were performed. The online database is built using in-house
438 script. Significantly differentially expressed epithelial and pneumococcal genes are listed in
439 **Supplementary Table 3** and **4**, respectively.

440 **qRT-PCR and quantitative fluorescence microscopy**

441 Infection studies were repeated, total RNA isolated and qRT-PCR is performed. For
442 fluorescence microscopy, infection studies were performed in 8-wells μ-slides (Ibidi, DE).
443 More in **Supplementary information**.

444 **Accession Numbers**

445 The raw data is accessible at http://www.ncbi.nlm.nih.gov/geo/ with accession number
446 GSE79595.

447

448 ## Author Contribution

449 R.A and J.W.V. designed the research, analyzed the data and wrote article. R.A performed
450 research, J.S analyzed the data, S.H. built online database.

451

452 ## Acknowledgements

453 We thank W.J. Quax and R. Setroikromo (UMCG, Groningen) for the human cell line, V.
454 Benes and B. Haase (GeneCore, EMBL, Heidelberg) for sequencing support, M. Kjos for
455 fruitful discussions and A. de Jong for bioinformatics support. We thank S. El Aidy and L.E.
456 Keller for comments on the manuscript. Work in Veening lab is supported by the EMBO
457 Young Investigator Program, VIDI fellowship (864.12.001) from the Netherlands
458 Organization for Scientific Research, Earth and Life Sciences (NWO-ALW), and ERC
459 Starting Grant 337399-PneumoCell.

460

461 ## Conflict of Interest

462 None

463

464 ## References

465 Abeyta, M., Hardy, G.G., and Yother, J. (2003). Genetic alteration of capsule type but not
466 PspA type affects accessibility of surface-bound complement and surface antigens of
467 *Streptococcus pneumoniae*. Infect. Immun. *71*, 218–225.

468 Attaiech, L., Olivier, A., Mortier-Barrière, I., Soulet, A.-L., Granadel, C., Martin, B., Polard,
469 P., and Claverys, J.-P. (2011). Role of the Single-Stranded DNA–Binding Protein SsbB in
470 Pneumococcal Transformation: Maintenance of a Reservoir for Genetic Plasticity. PLOS
471 Genet *7*, e1002156.

472 Avraham, R., Haseley, N., Brown, D., Penaranda, C., Jijon, H.B., Trombetta, J.J., Satija, R.,
473 Shalek, A.K., Xavier, R.J., Regev, A., et al. (2015). Pathogen Cell-to-Cell Variability Drives
474 Heterogeneity in Host Immune Responses. Cell *162*, 1309–1321.

475 Baddal, B., Muzzi, A., Censini, S., Calogero, R.A., Torricelli, G., Guidotti, S., Taddei, A.R.,
476 Covacci, A., Pizza, M., Rappuoli, R., et al. (2015). Dual RNA-seq of Nontypeable
477 *Haemophilus influenzae* and Host Cell Transcriptomes Reveals Novel Insights into Host-
478 Pathogen Cross Talk. mBio *6*, e01765–15.

479 Beiter, K., Wartha, F., Hurwitz, R., Normark, S., Zychlinsky, A., and Henriques-Normark, B.
480 (2008). The Capsule Sensitizes *Streptococcus pneumoniae* to α-Defensins Human
481 Neutrophil Proteins 1 to 3. Infect. Immun. *76*, 3710–3716.

482 Bidossi, A., Mulas, L., Decorosi, F., Colomba, L., Ricci, S., Pozzi, G., Deutscher, J., Viti, C.,
483 and Oggioni, M.R. (2012). A Functional Genomics Approach to Establish the Complement
484 of Carbohydrate Transporters in *Streptococcus pneumoniae* . PLoS ONE *7*, e33320.

485 Bogaert, D., De Groot, R., and Hermans, P.W.M. (2004). *Streptococcus pneumoniae*
486 colonisation: the key to pneumococcal disease. Lancet Infect. Dis. *4*, 144–154.

487 Bolger, A.M., Lohse, M., and Usadel, B. (2014). Trimmomatic: A flexible trimmer for Illumina
488 Sequence Data. Bioinformatics btu170.

489 Bootsma, H.J., Egmont-Petersen, M., and Hermans, P.W.M. (2007). Analysis of the In Vitro
490 Transcriptional Response of Human Pharyngeal Epithelial Cells to Adherent *Streptococcus*
491 *pneumoniae*: Evidence for a Distinct Response to Encapsulated Strains. Infect. Immun. *75*,
492 5489–5499.

493 Camilios-Neto, D., Bonato, P., Wassem, R., Tadra-Sfeir, M.Z., Brusamarello-Santos, L.C.,
494 Valdameri, G., Donatti, L., Faoro, H., Weiss, V.A., Chubatsu, L.S., et al. (2014). Dual RNA-
495 seq transcriptional analysis of wheat roots colonized by *Azospirillum brasilense* reveals up-
496 regulation of nutrient acquisition and cell cycle genes. BMC Genomics *15*, 378.

497 Carvalho, S.M., Kloosterman, T.G., Kuipers, O.P., and Neves, A.R. (2011). CcpA Ensures
498 Optimal Metabolic Fitness of *Streptococcus pneumoniae*. PLoS ONE *6*, e26707.

499 Choi, Y.-J., Aliota, M.T., Mayhew, G.F., Erickson, S.M., and Christensen, B.M. (2014). Dual
500 RNA-seq of Parasite and Host Reveals Gene Expression Dynamics during Filarial Worm–
501 Mosquito Interactions. PLOS Negl Trop Dis *8*, e2905.

502 Decramer, M., Janssens, W., and Miravitlles, M. (2012). Chronic obstructive pulmonary
503 disease. The Lancet *379*, 1341–1351.

504 Dennis, G., Sherman, B.T., Hosack, D.A., Yang, J., Gao, W., Lane, H.C., and Lempicki,
505 R.A. (2003). DAVID: Database for Annotation, Visualization, and Integrated Discovery.
506 Genome Biol. *4*, P3.

507 Dillon, L.A.L., Suresh, R., Okrah, K., Corrada Bravo, H., Mosser, D.M., and El-Sayed, N.M.
508 (2015). Simultaneous transcriptional profiling of *Leishmania major* and its murine
509 macrophage host cell reveals insights into host-pathogen interactions. BMC Genomics *16*,
510 1108.

511 Dobin, A., Davis, C.A., Schlesinger, F., Drenkow, J., Zaleski, C., Jha, S., Batut, P.,
512 Chaisson, M., and Gingeras, T.R. (2013). STAR: ultrafast universal RNA-seq aligner.
513 Bioinforma. Oxf. Engl. *29*, 15–21.

514 Forman, H.J., Zhang, H., and Rinna, A. (2009). Glutathione: Overview of its protective
515 roles, measurement, and biosynthesis. Mol. Aspects Med. *30*, 1–12.

516 Graham, R.M.A., and Paton, J.C. (2006). Differential Role of CbpA and PspA in Modulation
517 of In Vitro CXC Chemokine Responses of Respiratory Epithelial Cells to Infection with
518 *Streptococcus pneumoniae*. Infect. Immun. *74*, 6739–6749.

519 Gray, R.D., Duncan, A., Noble, D., Imrie, M., O'Reilly, D.S.J., Innes, J.A., Porteous, D.J.,
520 Greening, A.P., and Boyd, A.C. (2010). Sputum trace metals are biomarkers of
521 inflammatory and suppurative lung disease. Chest *137*, 635–641.

522 Hackett, N.R., Butler, M.W., Shaykhiev, R., Salit, J., Omberg, L., Rodriguez-Flores, J.L.,
523 Mezey, J.G., Strulovici-Barel, Y., Wang, G., Didon, L., et al. (2012). RNA-Seq quantification
524 of the human small airway epithelium transcriptome. BMC Genomics *13*, 82.

525 Hallstrand, T.S., Hackett, T.L., Altemeier, W.A., Matute-Bello, G., Hansbro, P.M., and
526 Knight, D.A. (2014). Airway epithelial regulation of pulmonary immune homeostasis and
527 inflammation. Clin. Immunol. Orlando Fla *151*, 1–15.

528 Hammerschmidt, S., Bergmann, S., Paterson, G.K., and Mitchell, T.J. (2007). Pathogenesis
529 of *Streptococcus pneumoniae* infections :adaptive immunity, innate immunity, cell biology,
530 virulence factors. In Community-Acquired Pneumonia, (Birkhäuser Basel), pp. 139–181.

531 Hussell, T., and Bell, T.J. (2014). Alveolar macrophages: plasticity in a tissue-specific
532 context. Nat. Rev. Immunol. *14*, 81–93.

533 Hvalbye, B.K.R., Aaberge, I.S., Løvik, M., and Haneberg, B. (1999). Intranasal
534 Immunization with Heat-Inactivated *Streptococcus pneumoniae* Protects Mice against
535 Systemic Pneumococcal Infection. Infect. Immun. *67*, 4320–4325.

536 Hyams, C., Camberlein, E., Cohen, J.M., Bax, K., and Brown, J.S. (2010). The
537 *Streptococcus pneumoniae* Capsule Inhibits Complement Activity and Neutrophil
538 Phagocytosis by Multiple Mechanisms. Infect. Immun. *78*, 704–715.

539 Jenner, R.G., and Young, R.A. (2005). Insights into host responses against pathogens from
540 transcriptional profiling. Nat. Rev. Microbiol. *3*, 281–294.

541 Jørgensen, M.G., van Raaphorst, R., and Veening, J.-W. (2013). Chapter 6 - Noise and
542 Stochasticity in Gene Expression: A Pathogenic Fate Determinant. In Methods in
543 Microbiology, C.H. and A. Wipat, ed. (Academic Press), pp. 157–175.

544 Kadioglu, A., Weiser, J.N., Paton, J.C., and Andrew, P.W. (2008). The role of
545 *Streptococcus pneumoniae* virulence factors in host respiratory colonization and disease.
546 Nat. Rev. Microbiol. *6*, 288–301.

547 Kash, J.C., Walters, K.-A., Davis, A.S., Sandouk, A., Schwartzman, L.M., Jagger, B.W.,
548 Chertow, D.S., Li, Q., Kuestner, R.E., Ozinsky, A., et al. (2011). Lethal synergism of 2009

549 pandemic H1N1 influenza virus and *Streptococcus pneumoniae* coinfection is associated
550 with loss of murine lung repair responses. mBio *2*.

551 Kietzman, C.C., Gao, G., Mann, B., Myers, L., and Tuomanen, E.I. (2016). Dynamic
552 capsule restructuring by the main pneumococcal autolysin LytA in response to the
553 epithelium. Nat. Commun. *7*, 10859.

554 Kjos, M., Aprianto, R., Fernandes, V.E., Andrew, P.W., van Strijp, J.A.G., Nijland, R., and
555 Veening, J.-W. (2015). Bright fluorescent *Streptococcus pneumoniae* for live-cell imaging of
556 host-pathogen interactions. J. Bacteriol. *197*, 807–818.

557 Korfhage, C., Wyrich, R., and Oelmuller, U. (2002). Ammonium sulfate for neutralization of
558 inhibitory effects (Google Patents).

559 Krisanaprakornkit, S., Weinberg, A., Perez, C.N., and Dale, B.A. (1998). Expression of the
560 peptide antibiotic human beta-defensin 1 in cultured gingival epithelial cells and gingival
561 tissue. Infect. Immun. *66*, 4222–4228.

562 Kröger, C., Colgan, A., Srikumar, S., Händler, K., Sivasankaran, S.K., Hammarlöf, D.L.,
563 Canals, R., Grissom, J.E., Conway, T., Hokamp, K., et al. (2013). An Infection-Relevant
564 Transcriptomic Compendium for *Salmonella enterica* Serovar Typhimurium. Cell Host
565 Microbe *14*, 683–695.

566 Kukurba, K.R., and Montgomery, S.B. (2015). RNA Sequencing and Analysis. Cold Spring
567 Harb. Protoc. *2015*, pdb.top084970.

568 Kumar, L., and E. Futschik, M. (2007). Mfuzz: A software package for soft clustering of
569 microarray data. Bioinformation *2*, 5–7.

570 Lee, H.-Y., Andalibi, A., Webster, P., Moon, S.-K., Teufert, K., Kang, S.-H., Li, J.-D.,
571 Nagura, M., Ganz, T., and Lim, D.J. (2004). Antimicrobial activity of innate immune
572 molecules against *Streptococcus pneumoniae, Moraxella catarrhalis* and nontypeable
573 *Haemophilus influenzae*. BMC Infect. Dis. *4*, 12.

574 Liao, Y., Smyth, G.K., and Shi, W. (2014). featureCounts: an efficient general purpose
575 program for assigning sequence reads to genomic features. Bioinforma. Oxf. Engl. *30*, 923–
576 930.

577 Livak, K.J., and Schmittgen, T.D. (2001). Analysis of relative gene expression data using
578 real-time quantitative PCR and the 2(-Delta Delta C(T)) Method. Methods San Diego Calif
579 *25*, 402–408.

580 Love, M.I., Huber, W., and Anders, S. (2014). Moderated estimation of fold change and
581 dispersion for RNA-seq data with DESeq2. Genome Biol. *15*, 550.

582 Lysenko, E.S., Lijek, R.S., Brown, S.P., and Weiser, J.N. (2010). Within-Host Competition
583 Drives Selection for the Capsule Virulence Determinant of *Streptococcus pneumoniae*.
584 Curr. Biol. *20*, 1222–1226.

585 Martin, B., Prudhomme, M., Alloing, G., Granadel, C., and Claverys, J.P. (2000). Cross-
586 regulation of competence pheromone production and export in the early control of
587 transformation in *Streptococcus pneumoniae*. Mol. Microbiol. *38*, 867–878.

588 Mlacha, S.Z.K., Romero-Steiner, S., Hotopp, J.C.D., Kumar, N., Ishmael, N., Riley, D.R.,
589 Farooq, U., Creasy, T.H., Tallon, L.J., and Liu, X. (2013). Phenotypic, genomic, and
590 transcriptional characterization of *Streptococcus pneumoniae* interacting with human
591 pharyngeal cells. BMC Genomics *14*, 383.

592 Nelson, A.L., Roche, A.M., Gould, J.M., Chim, K., Ratner, A.J., and Weiser, J.N. (2007).
593 Capsule enhances pneumococcal colonization by limiting mucus-mediated clearance.
594 Infect. Immun. *75*, 83–90.

595 Nicolas, P., Mäder, U., Dervyn, E., Rochat, T., Leduc, A., Pigeonneau, N., Bidnenko, E.,
596 Marchadier, E., Hoebeke, M., Aymerich, S., et al. (2012). Condition-dependent
597 transcriptome reveals high-level regulatory architecture in *Bacillus subtilis*. Science *335*,
598 1103–1106.

599 Ning, K., Fermin, D., and Nesvizhskii, A.I. (2012). Comparative analysis of different label-
600 free mass spectrometry based protein abundance estimates and their correlation with RNA-
601 Seq gene expression data. J. Proteome Res. *11*, 2261–2271.

602 van Opijnen, T., and Camilli, A. (2012). A fine scale phenotype-genotype virulence map of a
603 bacterial pathogen. Genome Res. *22*, 2541–2551.

604 Pedersen, M., Nissen, S., Mitarai, N., Svenningsen, S.L., Sneppen, K., and Pedersen, S.
605 (2011). The Functional Half-Life of an mRNA Depends on the Ribosome Spacing in an
606 Early Coding Region. J. Mol. Biol. *407*, 35–44.

607 Phipps, J.C., Aronoff, D.M., Curtis, J.L., Goel, D., O'Brien, E., and Mancuso, P. (2010).
608 Cigarette Smoke Exposure Impairs Pulmonary Bacterial Clearance and Alveolar
609 Macrophage Complement-Mediated Phagocytosis of *Streptococcus pneumoniae*. Infect.
610 Immun. *78*, 1214–1220.

611 Prina, E., Ranzani, O.T., and Torres, A. (2015). Community-acquired pneumonia. The
612 Lancet *386*, 1097–1108.

613 Rai, P., Parrish, M., Tay, I.J.J., Li, N., Ackerman, S., He, F., Kwang, J., Chow, V.T., and
614 Engelward, B.P. (2015). *Streptococcus pneumoniae* secretes hydrogen peroxide leading to
615 DNA damage and apoptosis in lung cells. Proc. Natl. Acad. Sci. *112*, E3421–E3430.

616 Rajam, G., Anderton, J.M., Carlone, G.M., Sampson, J.S., and Ades, E.W. (2008).
617 Pneumococcal surface adhesin A (PsaA): a review. Crit. Rev. Microbiol. *34*, 131–142.

618 Rose, M.C., and Voynow, J.A. (2006). Respiratory tract mucin genes and mucin
619 glycoproteins in health and disease. Physiol. Rev. *86*, 245–278.

620 Shelburne, S.A., Davenport, M.T., Keith, D.B., and Musser, J.M. (2008). The role of
621 complex carbohydrate catabolism in the pathogenesis of invasive streptococci. Trends
622 Microbiol. *16*, 318–325.

623 Siegel, S.J., Roche, A.M., and Weiser, J.N. (2014). Influenza promotes pneumococcal
624 growth during coinfection by providing host sialylated substrates as a nutrient source. Cell
625 Host Microbe *16*, 55–67.

626 Sorek, R., and Cossart, P. (2010). Prokaryotic transcriptomics: a new view on regulation,
627 physiology and pathogenicity. Nat. Rev. Genet. *11*, 9–16.

628 Soumelis, V., Reche, P.A., Kanzler, H., Yuan, W., Edward, G., Homey, B., Gilliet, M., Ho,
629 S., Antonenko, S., Lauerma, A., et al. (2002). Human epithelial cells trigger dendritic cell
630 mediated allergic inflammation by producing TSLP. Nat. Immunol. *3*, 673–680.

631 St-Pierre, C., Brochu, S., Vanegas, J.R., Dumont-Lagacé, M., Lemieux, S., and Perreault,
632 C. (2013). Transcriptome sequencing of neonatal thymic epithelial cells. Sci. Rep. *3*, 1860.

633 Talbot, T.R., Hartert, T.V., Mitchel, E., Halasa, N.B., Arbogast, P.G., Poehling, K.A.,
634 Schaffner, W., Craig, A.S., and Griffin, M.R. (2005). Asthma as a risk factor for invasive
635 pneumococcal disease. N. Engl. J. Med. *352*, 2082–2090.

636 Taniguchi, Y., Choi, P.J., Li, G.-W., Chen, H., Babu, M., Hearn, J., Emili, A., and Xie, X.S.
637 (2010). Quantifying *E. coli* proteome and transcriptome with single-molecule sensitivity in
638 single cells. Science *329*, 533–538.

639 Tecle, T., Tripathi, S., and Hartshorn, K.L. (2010). Review: Defensins and cathelicidins in
640 lung immunity. Innate Immun. *16*, 151–159.

641 The ENCODE Consortium (2011). Standards, Guidelines and Best Practices for RNA-Seq.
642 https://www.encodeproject.org/

643 Tseng, H.-J., McEwan, A.G., Paton, J.C., and Jennings, M.P. (2002). Virulence of
644 *Streptococcus pneumoniae*: PsaA mutants are hypersensitive to oxidative stress. Infect.
645 Immun. *70*, 1635–1639.

646 Valko, M., Leibfritz, D., Moncol, J., Cronin, M.T.D., Mazur, M., and Telser, J. (2007). Free
647 radicals and antioxidants in normal physiological functions and human disease. Int. J.
648 Biochem. Cell Biol. *39*, 44–84.

649 Vogel, C., and Marcotte, E.M. (2012). Insights into the regulation of protein abundance from
650 proteomic and transcriptomic analyses. Nat. Rev. Genet. *13*, 227–232.

651 Voynow, J.A., and Rubin, B.K. (2009). Mucins, Mucus, and Sputum. Chest *135*, 505–512.

652 Wagner, G.P., Kin, K., and Lynch, V.J. (2012). Measurement of mRNA abundance using
653 RNA-seq data: RPKM measure is inconsistent among samples. Theory Biosci. Theor. Den
654 Biowissenschaften *131*, 281–285.

655 Westermann, A.J., Gorski, S.A., and Vogel, J. (2012). Dual RNA-seq of pathogen and host.
656 Nat. Rev. Microbiol. *10*, 618–630.

657 Westermann, A.J., Förstner, K.U., Amman, F., Barquist, L., Chao, Y., Schulte, L.N., Müller,
658 L., Reinhardt, R., Stadler, P.F., and Vogel, J. (2016). Dual RNA-seq unveils noncoding RNA
659 functions in host-pathogen interactions. Nature *529*, 496–501.

660 Yesilkaya, H., Manco, S., Kadioglu, A., Terra, V.S., and Andrew, P.W. (2008). The ability to
661 utilize mucin affects the regulation of virulence gene expression in *Streptococcus*
662 *pneumoniae*. FEMS Microbiol. Lett. *278*, 231–235.

Zahlten, J., Kim, Y.-J., Doehn, J.-M., Pribyl, T., Hocke, A.C., García, P., Hammerschmidt, S., Suttorp, N., Hippenstiel, S., and Hübner, R.-H. (2015). *Streptococcus pneumoniae*-Induced Oxidative Stress in Lung Epithelial Cells Depends on Pneumococcal Autolysis and Is Reversible by Resveratrol. J. Infect. Dis. *211*, 1822–1830.

Figures and Legends

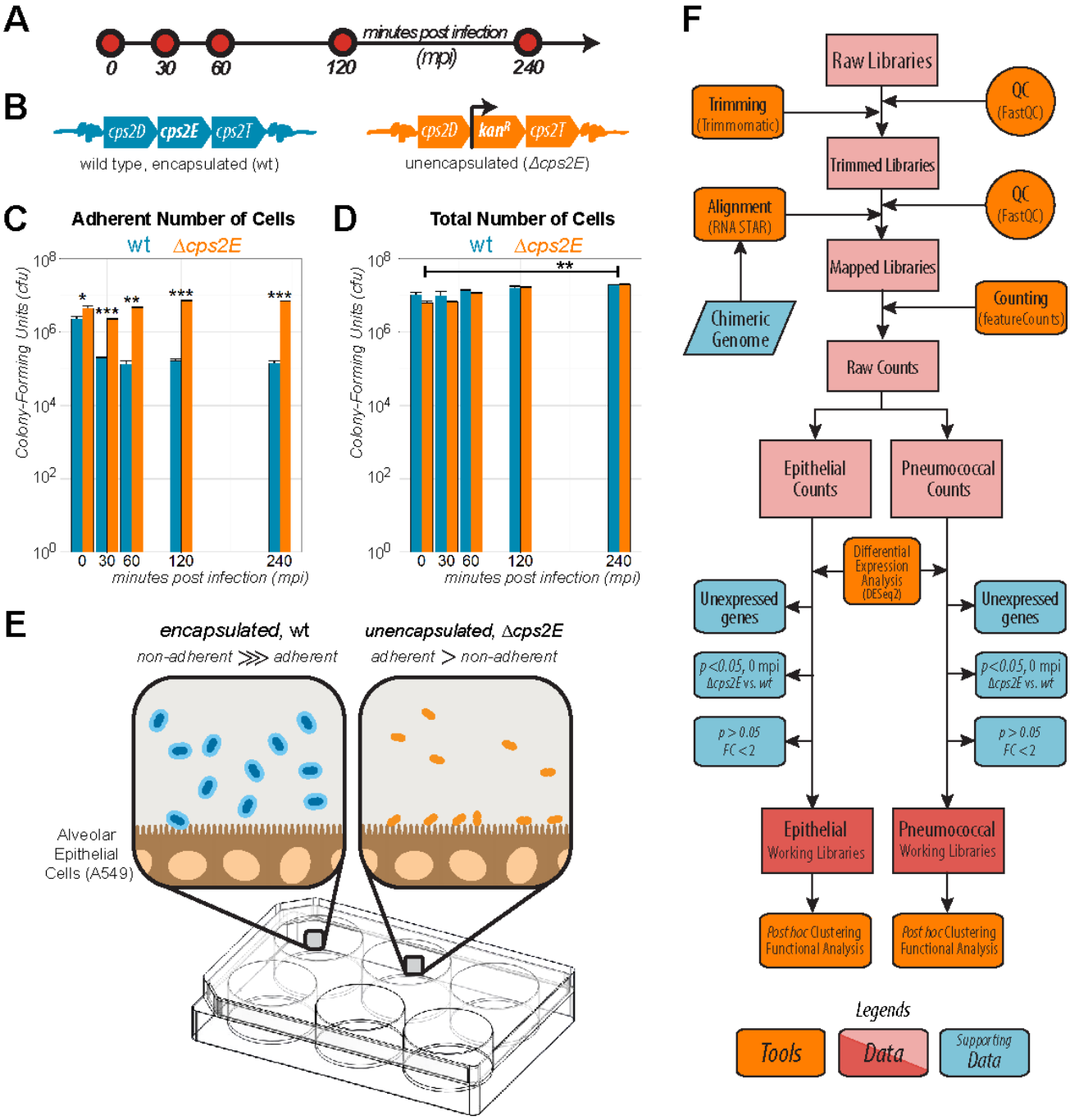

Figure 1. The early infection model. Confluent monolayer of alveolar epithelial cell line

(A549) was co-incubated with *S. pneumoniae* strain D39. **A**. We chose five infection time points: 0, 30, 60, 120 and 240 minutes post infection (mpi). **B**. Since adherence is a hallmark of infection, we used an unencapsulated strain, created by disrupting *cps2E* vital in capsule biogenesis. **C**. Δ*cps2E* strain adhered more readily to epithelial cells than its encapsulated parental strain. 30 mpi, Δ*cps2E* (orange bar) showed significantly ($p<0.001$) more adherent cells than its parental strain (cyan bar). Data is presented as mean±SEM. **D**. At 240 mpi, both strains multiplied significantly ($p<0.01$) with no significant difference between strains. **E**. Encapsulated strain has more free-floating than adherent cells while Δ*cps2E* has a higher fraction of adherent bacteria. **F**. After quality-check, low-quality reads were trimmed. Reads were aligned to a synthetic chimeric genome. Aligned reads were counted and classified as epithelial or as pneumococcal counts. We removed three gene fractions, clustered and performed functional enrichment to the working libraries.

670

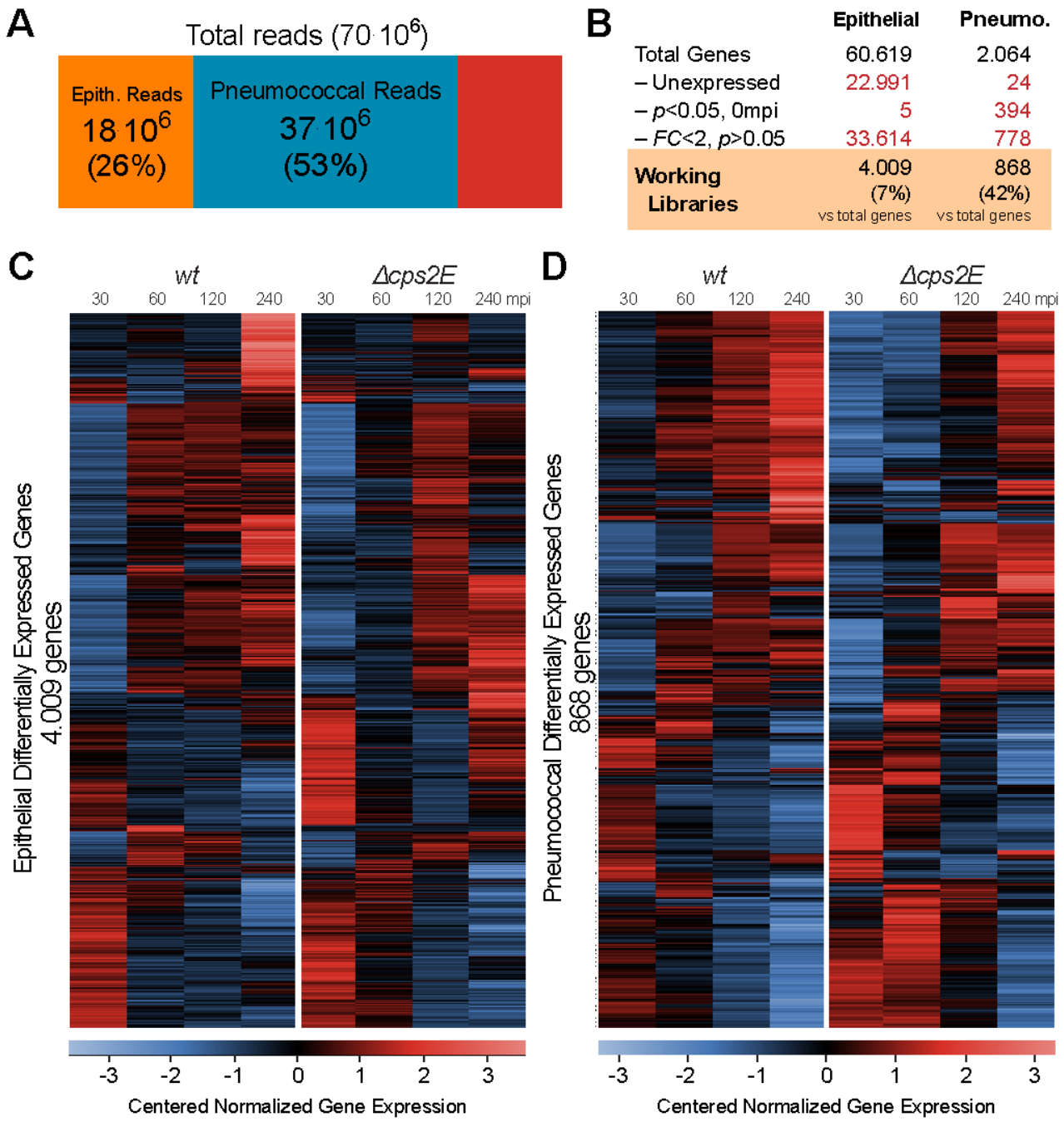

Fig.2. Dual RNA-Seq generates high-quality datasets suitable for probing host-pathogen transcriptomes. A. On average, there are 70 million reads per library: 18 million reads were mapped to the human genome while 37 million reads to pneumococcal genome. **B.** We excluded three gene fractions: unexpressed genes, i.e.: without counts in any libraries; genes that were differentially expressed at 0 mpi ($p<0.05$) between Δ*cps2E*

and wt libraries and genes with no statistical significance (p>0.05) and fold change less than two (FC<2) in all contrast. Epithelial working libraries contain 4.009 genes (7% of human genes) while pneumococcal working libraries 868 genes (42% pneumococcal genes). **C.** Gene expression in epithelial working libraries were normalized, centered and automatically clustered. The left panel shows epithelial genes in response to encapsulated strain while the right panel shows epithelial response to Δ*cps2E S. pneumoniae* at different time points. Clear clusters of co-expressed epithelial genes can be observed in the heat map. Blue indicates a relatively lower expression while red, a higher value. **D**. Correspondingly, we presented pneumococcal expression in the same manner: left panel shows wild type pneumococcal response to epithelial cells, while right panel shows Δ*cps2E* response.

671

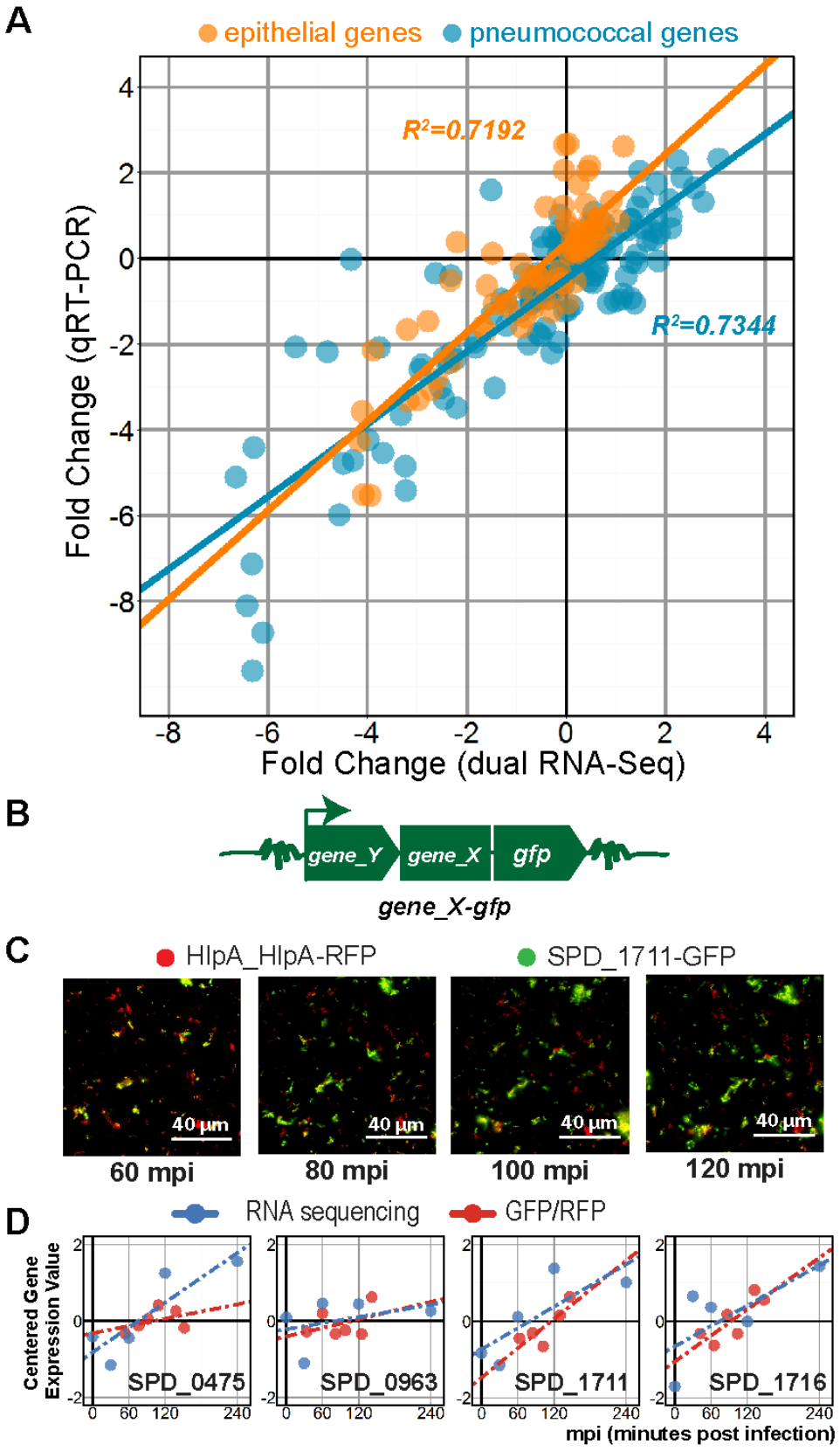

Fig.3. Validation of dual RNA-Seq. A. We confirmed dual RNA-Seq gene expression

values by qRT-PCR. The infection study was repeated in duplicates and total RNA was isolated as previously. Ten human and 19 pneumococcal genes were chosen as validation targets. We plotted fold changes from qRT-PCR against dual RNA-Seq fold changes and observed a high degree of correlation ($R^2 > 0.7$, Pearson) for both species. **B.** We also confirmed pneumococcal gene expression at the protein level by quantitative fluorescence microscopy. Four target genes (SPD_0475, SPD_0963, SPD_1711 and SPD_1716) were C-terminally tagged with GFP at their own locus. GFP-fusion were performed in the Δ*cps2E* strain expressing RFP fused to HlpA. **C.** Non-deconvolved image of SPD_1711-GFP in Δ*cps2E* strain up to 120 mpi. While RFP emitted a relatively constant signal, the GFP signal increases. **D**. We plotted dual RNA-Seq expression values superimposed to the GFP/RFP ratio. To some extent, transcriptional changes corresponded to protein expression.

672

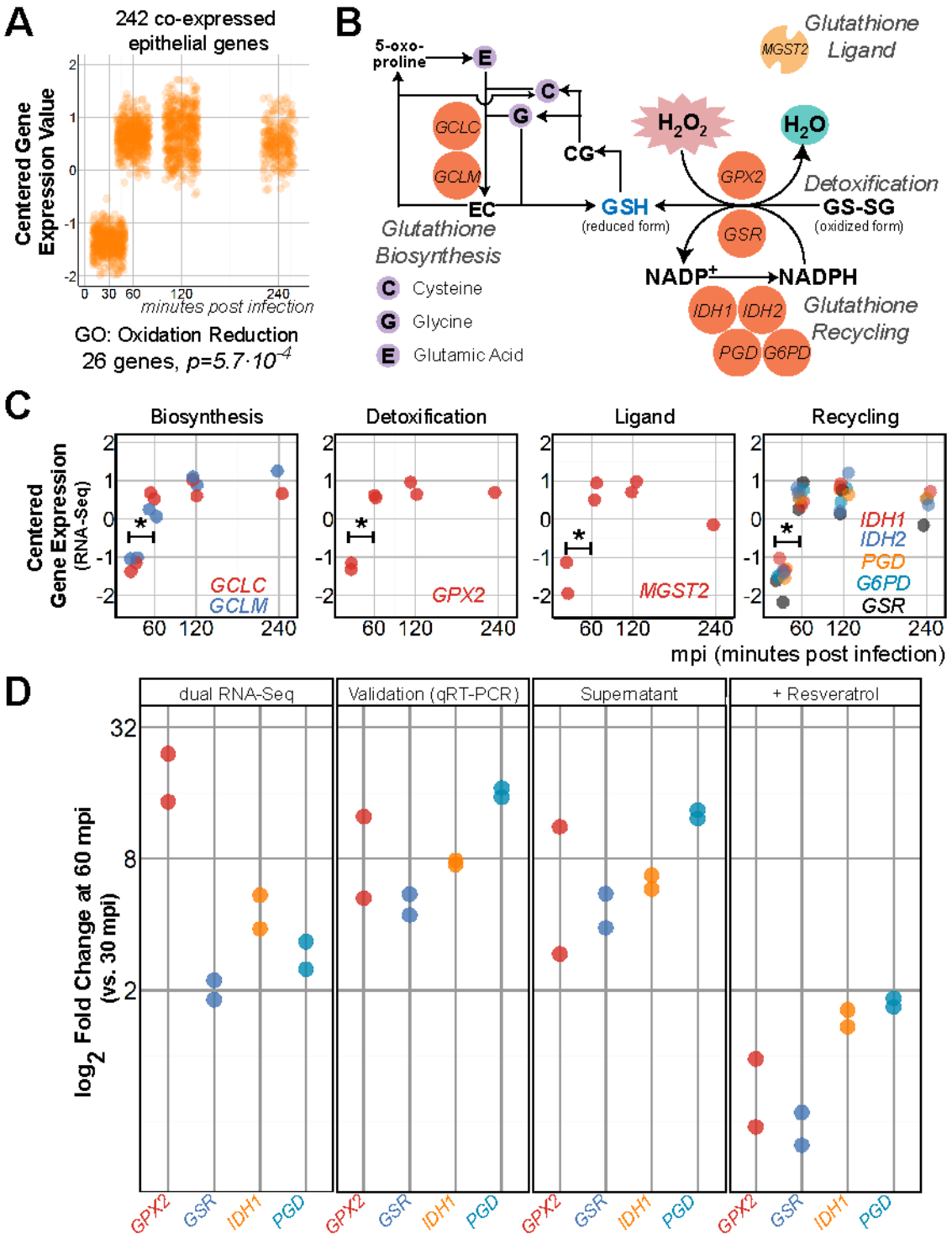

Fig.4. Epithelial glutathione-associated genes are activated in response to pneumococcal ROS. A. We clustered epithelial working libraries exposed to wild type pneumococci and found a cluster of 242 co-expressed genes showing sustained upregulation (p<0.05, FC>2) at 60 mpi compared to 30 mpi. GO analysis showed that

“oxidation reduction” was enriched in 26 genes (p=5.7·10^{-4}). **B**. Nine genes from the subset are associated with glutathione (GSH), an important antioxidant. Main glutathione-associated processes are biosynthesis of glutathione, detoxification of ROS assisted by ligand and glutathione recycling. **C**. Between 30 and 60 mpi, *GCLC* was increased 2.3±1.1 times and *GCLM* 2.4±1.2 times. *GPX2*, the main detoxification gene was activated 18.7±1.3 times while the ligand, *MGST2* 3.2±1.2 times. Genes involved in the recycling of glutathione were activated: *IDH1,* 4.6±1.2; *IDH2*, 2.4±1.2; *PGD,* 2.9±1.2; *G6PD,* 6.6±1.2 and *GSR,* 2.0±1.1 times. **D**. We validated *GPX2*, *GSR, IDH1* and *PGD* expression with qRT-PCR. Epithelial incubation with pneumococcal supernatant showed similar upregulation of glutathione-associated genes. Addition of resveratrol (100μM) into the model diminished the upregulation (*FC*<2) altogether.

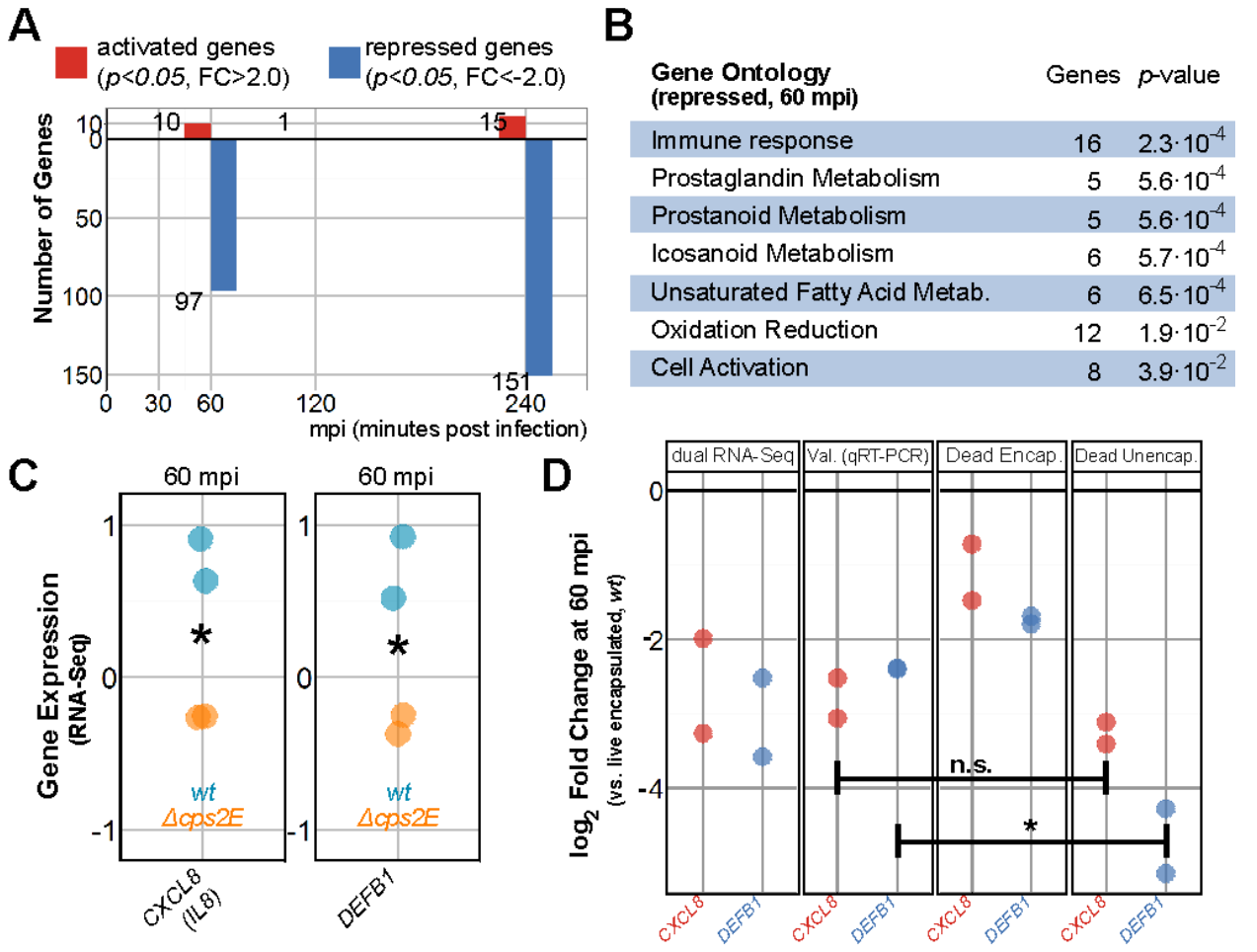

Fig.5. Adherent *S. pneumoniae* repress epithelial innate immune responses. A. At 60 mpi, 97 epithelial genes were significantly repressed upon exposure to Δ*cps2E* bacteria compared to exposure to wild type pneumococci. **B.** GO term enrichment to 60 mpi repressed genes resulted in "immune response" (16 genes, $p=2.3\cdot10^{-4}$), prostaglandin metabolism (5 genes, $p=5.6\cdot10^{-4}$) and oxidation reduction (12 genes, $p=0.019$) among others. **C.** Δ*cps2E*–exposed epithelial cells expressed 2.6±1.3 fold less *CXCL8* and 3.0±1.2 fold less *DEFB1* than wild type-exposed epithelial cells. **D.** We validated *CXCL8* and *DEFB1* repression by qRT-PCR. Heat-inactivated encapsulated bacteria showed no repression of *CXCL8* and *DEFB1,* i.e., no difference ($p>0.05$) compared to viable encapsulated *S. pneumoniae* (Dead Encap.). While infection with heat-inactivated Δ*cps2E* repressed *CXCL8* to the level of viable Δ*cps2E*, *DEFB1* was more repressed ($p<0.05$) by

dead Δ*cps2E* than by viable unencapsulated pneumococci.

673

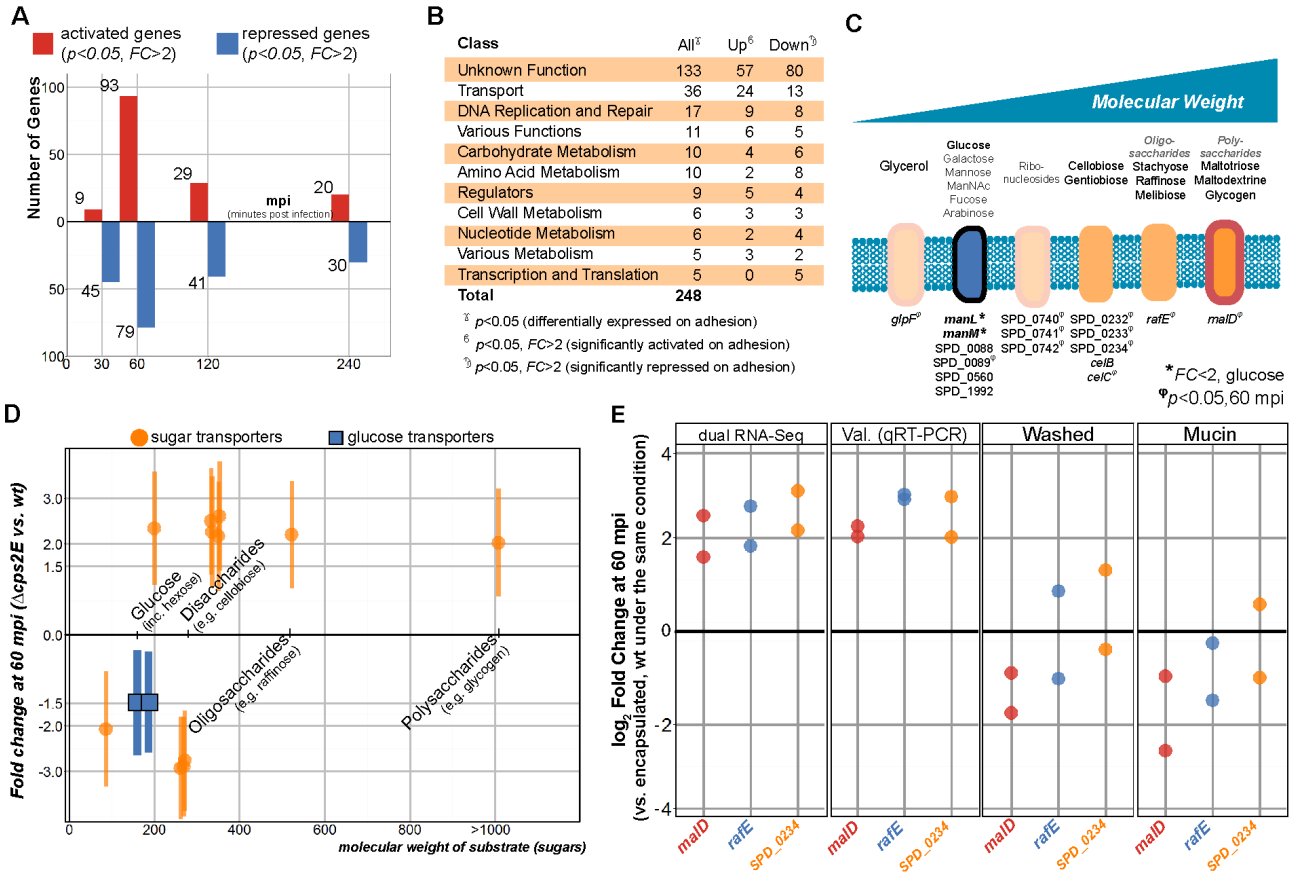

Fig.6. Adherent pneumococci gain access to host-derived carbohydrates and activate non-glucose sugar importers. A. 248 genes were differentially expressed between pneumococcal strains exposed to epithelial cells: 115 genes of the 248 genes were activated in Δ*cps2E* compared to wt pneumococci while 138 genes were repressed. Note that five genes showed activation and repression at different time points. **B.** Most of the differentially-expressed genes are of unknown function (133 genes, 54% of 248), followed by cellular transport (36 genes, 15%) and DNA replication, repair and recombination (17 genes, 7%). **C.** 15 of the 36 transporter genes are described to transport carbohydrate. The carbohydrate-importers transport a wide range of carbohydrates, from

simple monosaccharides to complex polysaccharides. **D.** At 60 mpi, the expression of glucose transporters (*manLM*, blue boxes) is repressed ($p<0.05$, $FC=1.5$) in Δ*cps2E* compared to encapsulated *S. pneumoniae*. Seven non-glucose transporters are activated ($p<0.05$, $FC>2$) in the Δ*cps2E* strain: SPD_0089, *celC,* SPD_0232/33/34*, rafE* and *malD*. **E.** We validated the data by qRT- PCR for three sugar importers: *malD* (polysaccharides)*, rafE* (oligosaccharide), and SPD_0234 (non-glucose disaccharide). By removing epithelial mucus prior to infection, the importers were no longer activated in Δ*cps2E* compared to wild type ($FC<2$, Washed). Incubation with type III porcine mucin ($5 g \cdot L^{-1}$) did not activate the genes in Δ*cps2E* compared to encapsulated pneumococci ($FC<2$).

674